Journal of *Physica Scripta*

PAPER

Crossmark

RECEIVED
dd Month Year

REVISED
dd Month Year

ACCEPTED
dd Month Year

PUBLISHED
dd Month Year

Doppler effects on two-photon Rydberg spectroscopy in counter- and co-propagating configurations

Han Jiaofeng[1], Yang Baodong[1,2,3,*], Wang Yubo[1], Ruan Jingge[1], and Wang Junmin[2,3]

[1] *College of Physics and Electronic Engineering, Shanxi University, Taiyuan 030006, China*
[2] *State Key Laboratory of Quantum Optics Technologies and Devices, and Institute of Opto-Electronics, Shanxi University, Taiyuan 030006, China*
[3] *Collaborative Innovation Center of Extreme Optics, Shanxi University, Taiyuan 030006, China*

*Author to whom any correspondence should be addressed.

E-mail: ybd@sxu.edu.cn

Keywords: Rydberg atoms, electromagnetically induced transparency, four-wave mixing

Abstract

We investigate Rydberg electromagnetically induced transparency (EIT) spectroscopy in a ladder-type cesium $6S_{1/2} \rightarrow 6P_{3/2} \rightarrow nD$ system, driven by an 852 nm probe field and a 510 nm coupling field. The dependence of the Rydberg EIT spectra on the probe detuning is systematically analyzed by resolving the contributions from different atomic velocity groups. Exploiting the Doppler effect and the resulting velocity-selective spectral response, an intrinsic frequency ruler is established for directly measuring Rydberg EIT spectral intervals without external frequency calibration, thereby simplifying the experimental setup. Furthermore, we compare the spectral characteristics obtained with counter- and co-propagating probe and coupling beams. The counter-propagating configuration is essential for achieving narrow linewidth, high signal-to-noise-ratio Rydberg EIT spectroscopy in a ladder-type atomic system with a probe wavelength longer than the coupling wavelength. Remarkably, well-resolved Rydberg spectra are also observed in the co-propagating configuration, providing an alternative route to two-photon Rydberg spectroscopy, especially for the ladder-type systems in which the probe wavelength is shorter than the coupling wavelength. In such inverted systems, ladder-type EIT signals are strongly suppressed by Doppler mismatch.

1. Introduction

Rydberg atoms, in which a valence electron is excited to a state with a high principal quantum number ($n \gg 1$), exhibit remarkable properties such as large transition dipole moments ($\sim n^2$), long radiative lifetimes ($\sim n^3$), and giant polarizabilities ($\sim n^7$). These features make them highly sensitive to external electromagnetic fields and give rise to strong dipole-dipole interactions [1]. Consequently, Rydberg atoms have attracted considerable interest in a wide range of applications, including quantum information processing, quantum simulation, and precision measurements of electromagnetic fields [2-4]. In these applications, the achievable sensitivity and spectral resolution are largely determined by the signal-to-noise ratio (SNR) and linewidth of the measured Rydberg spectra. Therefore, improving the spectral SNR and suppressing linewidth broadening remain central issues in Rydberg spectroscopy [5-7]. Most Rydberg spectroscopy experiments employ a two-photon stepwise excitation scheme, in which atoms are excited from the ground state to a Rydberg state via an intermediate state, and the corresponding spectral response is detected through electromagnetically induced transparency (EIT). In early Rydberg EIT experiments, spectra are typically obtained by scanning the frequency of probe laser. In thermal atomic vapor, however, Doppler background degrades the spectral SNR and limits measurement precision [8]. Subsequently, Doppler background-free EIT spectra in ladder-type systems have been realized by fixing the probe frequency and scanning the coupling-laser frequency [9-12]. Furthermore, substantial efforts

© Year Copyright holder

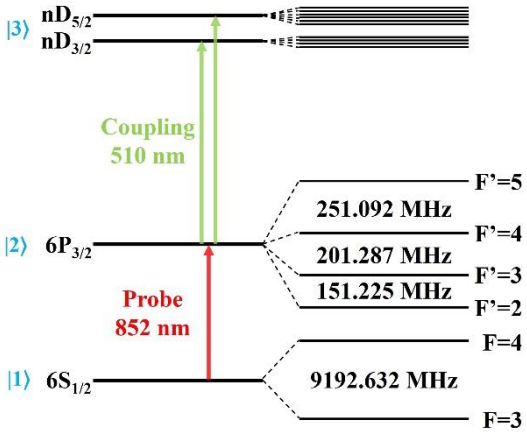


Figure 1. Energy-level diagram of the ladder-type Rydberg EIT in cesium.

have been devoted to enhancing the quality of Rydberg EIT spectra by optimizing the polarization combination of the probe and coupling beams and their spatial intensity distributions [6, 13, 14], by introducing an additional repumping field [15, 16], and by incorporating optical cavities, which can significantly improve the SNR while preserving the narrow-linewidth characteristic of Rydberg EIT spectra [17-19]. Recently, double-resonance optical-pumping polarization spectroscopy has been extended to Rydberg states, enabling the observation of Rydberg EIT polarization spectra and modulation-free locking of the coupling laser to the intermediate-to-Rydberg transition [14]. Beyond the conventional two-photon excitation scheme, Rydberg spectra have also been obtained using single-photon excitation [20, 21], three-photon EIT [22], and four-wave mixing [23]. More recently, the Autler-Townes (A-T) splitting has been exploited for Rydberg spectroscopy [24].

In practical applications such as Rydberg-atom-based microwave electric-field sensing, determination of A-T splitting intervals often requires an external frequency reference, typically provided by acousto-optic modulator (AOM) or electro-optic modulator (EOM) and so on, and various calibration techniques have therefore been developed to improve measurement accuracy [25, 26]. Nevertheless, these auxiliary calibration tools increase the complexity of the experimental system. Meanwhile, Rydberg EIT experiments generally employ counter-propagating probe and coupling beams to suppress Doppler broadening [10-17]. However, Rydberg spectra in the co-propagating configuration have received considerably less attention [27, 28]. Recent experimental results reported in 2026, however, have shown that the enhanced Doppler effect in this geometry can be exploited to improve the sensitivity of Rydberg-atom-based microwave receivers [29].

In this work, we investigate the effects of probe frequency detuning and atomic velocity on the Rydberg EIT in the cesium (^{133}Cs) $6S_{1/2} \rightarrow 6P_{3/2} \rightarrow$ nD ladder-type system. Velocity-dependent spectral features allow the establishment of an intrinsic frequency ruler, enabling direct measurement of frequency intervals in the Rydberg spectra without external frequency references. We further compare co-propagating and counter-propagating excitation schemes and characterize the dependence of spectral amplitude and linewidth on the coupling power. These results offer valuable guidance for further applications in precision spectroscopy and Rydberg-atom-based sensing.

2. Theory and experimental setup

The experiment is based on the ^{133}Cs $6S_{1/2} \rightarrow 6P_{3/2} \rightarrow$ nD ladder-type system, as shown in Figure 1. The intermediate excited state $6P_{3/2}$ has a natural linewidth of 5.22 MHz and is split into four hyperfine levels, F' = 2, 3, 4, and 5, with adjacent frequency intervals of 151.225,

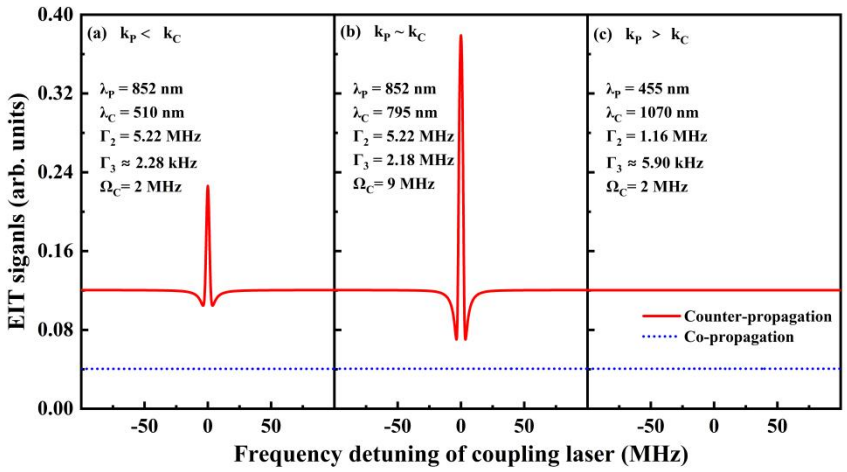


Figure 2. Theoretical EIT spectra in counter- and co-propagating beam configurations for different probe and coupling wavelength relationships: (a) $\lambda_P > \lambda_C$, (b) $\lambda_P \sim \lambda_C$, (c) $\lambda_P < \lambda_C$. The Cs vapor temperature is T = 300 K, and probe frequency detuning $\Delta_p = 0$.

201.287, and 251.092 MHz, respectively. The natural linewidth of the Rydberg nD state is on the order of 1-5 kHz [7]. Due to the large principal quantum number n, the hyperfine splitting of the Rydberg state is significantly reduced and can usually be treated approximately as degenerate. The ground state $6S_{1/2}$, the intermediate excited state $6P_{3/2}$, and the Rydberg state nD are denoted as $|1\rangle$, $|2\rangle$, and $|3\rangle$, respectively. A weak probe field at 852 nm, with angular frequency ω_p and Rabi frequency Ω_p, drives the $|1\rangle \rightarrow |2\rangle$ transition, while a strong coupling field at 510 nm, with angular frequency ω_c and Rabi frequency Ω_c, drives the $|2\rangle \rightarrow |3\rangle$ transition. The frequency detunings of the probe and coupling fields are defined as follows:

$$\Delta_p = \omega_p - \omega_{21}\,,\ \Delta_c = \omega_c - \omega_{32} \tag{1}$$

where ω_{ij} denotes the transition frequency between the corresponding atomic states. Under the rotating-wave approximation, the atom-field interaction Hamiltonian, H_{int}, is given by [13]:

$$H_{int} = \begin{bmatrix} 0 & \frac{\hbar}{2}\Omega_p & 0 \\ \frac{\hbar}{2}\Omega_p & -\hbar\Delta_p & \frac{\hbar}{2}\Omega_c \\ 0 & \frac{\hbar}{2}\Omega_c & -\hbar\delta \end{bmatrix} \tag{2}$$

where $\hbar$ is the reduced Planck constant and $\delta = \Delta_p + \Delta_c$ denotes the two-photon detuning. Substituting H_{int} into the density-matrix equation of motion yields:

$$\dot{\rho} = -\frac{\mathrm{i}}{\hbar}[H_{int}, \rho] + \mathcal{L} \tag{3}$$

where $\mathcal{L}$ accounts for the relaxation and dephasing processes in the system. The steady-state density-matrix elements can then be obtained by setting $d\rho/dt = 0$. In the weak-probe approximation ($\Omega_p \ll \Omega_c$), $\rho_{22} \approx \rho_{33} \approx 0$ and $\rho_{11} \approx 1$, and the susceptibility can be expressed as follows [30]:

$$\chi(v)dv = \frac{4i\hbar g_{21}^2/\varepsilon_0}{\gamma_{21} - i\Delta_p - i\frac{\omega_p}{c}v + \frac{\Omega_c^2/4}{\gamma_{31} - i(\Delta_p + \Delta_c) - i(\omega_p \pm \omega_c)v/c}} N(v)dv \tag{4}$$

where g_{21} is the dipole transition matrix element, γ_{ij} denotes the coherence relaxation rate between the relevant atomic levels, ε_0 is the vacuum permittivity, c is the speed of light, v is the atomic velocity component along the propagation direction of the 852 nm probe beam, and $N(v)$ is the one-dimensional Maxwell velocity distribution. When the probe and coupling beams interact with the atoms in a counter-propagating geometry, the term $-i(\omega_p \pm \omega_c)v/c$ in equation (4) takes the "-" sign, corresponding to a near-Doppler-free configuration [31]. In contrast, for

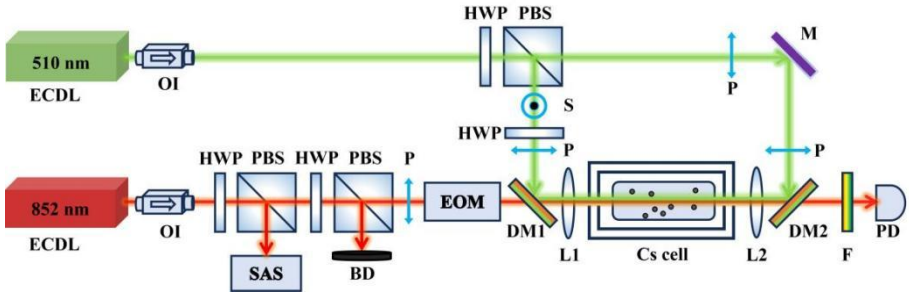


Figure 3. Schematic diagram of experimental setup for Rydberg spectra in counter- and co-propagating beam configurations (OI, optical isolator; HWP, half-wave plate; PBS, polarizing beam splitter; M, mirror; DM, dichroic mirror; L, achromatic lens; PD, photodetector; F, 852 nm filter; SAS, saturated absorption spectroscopy; BD, beam dump; EOM, electro-optic modulator; S, s polarization; P, p polarization)

the co-propagating geometry, the "+" sign should be taken, leading to a larger Doppler broadening because the Doppler shifts experienced by moving atoms for the probe and coupling lasers contribute in the same direction. To facilitate the subsequent discussion of the experimental results, the Doppler-averaged probe transmission signals are simulated by integrating over the one-dimensional Maxwell–Boltzmann velocity distribution based on equation (4) for three representative cases: (a) $\lambda_P > \lambda_C$, (b) $\lambda_P \approx \lambda_C$, and (c) $\lambda_P < \lambda_C$. To bring the theoretical results into closer agreement with experimental observations, three representative ladder-type energy-level schemes in ^{133}Cs are selected: $6S_{1/2} \rightarrow 6P_{3/2} \rightarrow 50D_{3/2(5/2)}$ (852 nm + 510 nm) as this work, $6S_{1/2} \rightarrow 6P_{3/2} \rightarrow 8S_{1/2}$ (852 nm + 795 nm) [9], and $6S_{1/2} \rightarrow 7P_{3/2} \rightarrow 32S_{1/2}$ (455 nm + 1070 nm) [32], which approximately correspond to the above three cases, respectively. The calculated results indicate that the Rydberg EIT signal can be observed under the counter-propagating configuration in the case that $\lambda_P > \lambda_C$. Notably, for the case of $\lambda_P < \lambda_C$, the "EIT" feature becomes hardly distinguishable from the background in both the co- and counter-propagating configurations [32, 33], as illustrated in figure 2.

The experimental setup is shown in figure 3. The 852 nm probe and 510 nm coupling beams are generated by external-cavity diode lasers (ECDLs), both with linewidths below ~1 MHz. The probe laser is locked to the ^{133}Cs $6S_{1/2}(F=4) \rightarrow 6P_{3/2}(F'=5)$ transition using saturated absorption spectroscopy (SAS), while the coupling laser, with an available power of ~30 mW, is scanned across the $6P_{3/2}(F'=5) \rightarrow$ nD transition. Under the two-photon resonance condition ($\Delta_p + \Delta_c \approx 0$), destructive quantum interference prepares the atoms in a dark state, resulting in a narrow EIT transmission window. The 510 nm coupling beam is split by a half-wave plate (HWP) and a polarizing beam splitter (PBS). The reflected beam is combined with the probe beam by a dichroic mirror (DM1) and enters the Cs cell in the co-propagating configuration. The transmitted beam is redirected by a mirror (M) and a second dichroic mirror (DM2), and then counter-propagates with the probe beam through the same Cs cell. To ensure a consistent comparison of the Rydberg spectra in the co- and counter-propagating configurations, the polarization combinations for the probe and coupling beams are kept identical by inserting an HWP into the optical path before the DM1. Before entering the Cs cell, the probe beam is phase-modulated by an EOM to generate radio-frequency (RF) sidebands for frequency calibration. The two beams are focused at the center of the Cs cell by a confocal optical system consisting of two achromatic lenses (L1 and L2) with focal lengths of 75 mm, producing a beam waist diameter of ~50 μm. The Cs cell is 20 mm in length and 25 mm in diameter. At room temperature (~300 K), the atomic number density is approximately 10^{10}-10^{11} cm^{-3}. To minimize stray magnetic fields, the Cs cell is enclosed in μ-metal shielding. After passing through the Cs cell, the probe beam is separated from the coupling beam by DM2, and the residual 510 nm light is removed with an 852 nm bandpass filter (F). The transmitted probe

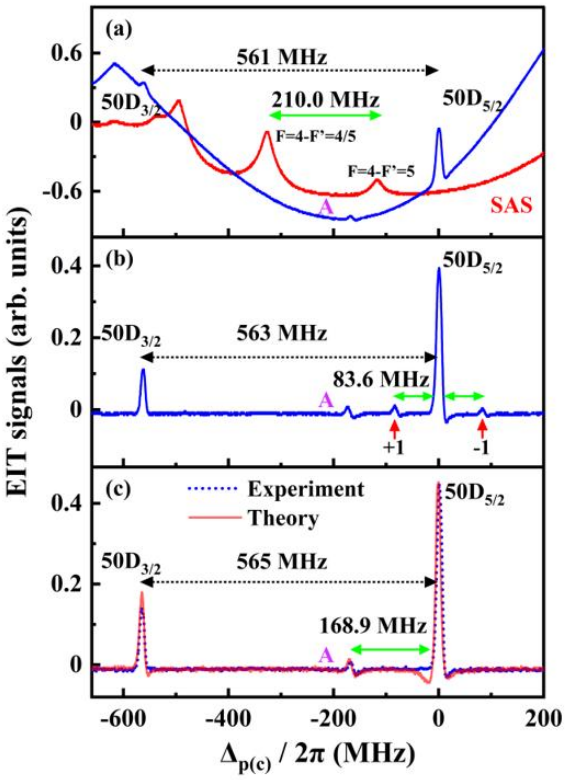


Figure 4. Rydberg EIT spectra of the ^{133}Cs $6P_{3/2}(F'=5) \rightarrow 50D_{3/2}$ / $50D_{5/2}$ transitions. (a) EIT spectrum with Doppler background obtained by scanning the probe laser frequency; (b) Doppler background-free EIT spectrum obtained by applying a 50 MHz RF modulation signal to the probe laser at a fixed frequency; (c) Doppler background-free EIT spectrum with the probe laser frequency fixed.

signal is detected by a silicon avalanche photodetector (Thorlabs APD440A) to record the Rydberg spectra.

3. Experimental results and discussion

3.1. Rydberg EIT spectral characteristics and intrinsic frequency scale

Figure 4 shows typical Rydberg EIT spectra obtained in the counter-propagating configuration, with the powers of the 852 nm probe and 510 nm coupling beams set to 2.8 μW and 30 mW, respectively. Three experimental methods for establishing the frequency scale are also demonstrated. Figure 4(a) presents the Rydberg EIT spectra obtained using the conventional EIT scanning scheme, in which the probe frequency is scanned across the $6S_{1/2}(F=4) \rightarrow 6P_{3/2}$ transitions, while the coupling frequency is fixed near the $6P_{3/2} \rightarrow 50D$ transition. Since the probe frequency is scanned, the measured Rydberg EIT spectra are superimposed on a Doppler-broadened background, which can hinder accurate determination of the spectral line positions. However, an advantage of this scanning scheme is that the SAS signal of the $6S_{1/2}(F=4) \rightarrow 6P_{3/2}$ transition can be recorded simultaneously and used as a frequency reference. The known 125.5 MHz interval between the $6S_{1/2}(F=4) \rightarrow 6P_{3/2}(F'=5)$ and $6S_{1/2}(F=4) \rightarrow 6P_{3/2}(F'=4/5)$ spectral lines in the SAS is used as the frequency reference. Accounting for the wavelength mismatch between the probe and coupling beams, this interval corresponds to an effective calibration interval of 125.5 × 852.356 / 509.627 = 210.0 MHz in the Rydberg EIT spectra. Accordingly, the separation between the $6P_{3/2}(F'=5) \rightarrow 50D_{3/2}$ and $6P_{3/2}(F'=5) \rightarrow 50D_{5/2}$ Rydberg EIT resonances is measured to be 561 ± 9 MHz, corresponding to

the fine-structure splitting of the 50D Rydberg state [34]. Here, the uncertainty represents the standard deviation of repeated measurements.

Figure 4(b) shows the Rydberg EIT spectra obtained when the probe frequency is locked to the $6S_{1/2}(F=4) \rightarrow 6P_{3/2}(F'=5)$ hyperfine transition using the SAS signal, while the coupling frequency is scanned across the $6P_{3/2} \rightarrow 50D$ transition. Since the probe frequency is kept fixed, the Rydberg EIT spectra exhibit a flat background, significantly improving the SNR. To calibrate the frequency axis of the Rydberg EIT spectra, a 50 MHz RF modulation signal is applied to the 852 nm probe beam using an EOM. Experimentally, the corresponding ± 1st-order sideband EIT signals are clearly observed on both sides of the $6P_{3/2}(F'=5) \rightarrow 50D_{5/2}$ EIT peak. Due to the wavelength mismatch, the frequency interval between each sideband signal and the main EIT peak for the same transition is 50.0 × 852.356 / 509.627 = 83.6 MHz. Using this interval as the frequency reference, the fine-structure splitting of the 50D level is determined to be approximately 563 ± 6 MHz.

Figure 4(c) shows Rydberg EIT spectra with a flat background obtained without applying RF modulation. In addition to the two main EIT peaks associated with the $50D_{3/2}$ and $50D_{5/2}$ states, a weak EIT peak, labelled A, appears between them. This peak A arises from velocity-selective excitation of thermal atoms. At room temperature, cesium atoms in the vapor cell follow a one-dimensional Maxwell-Boltzmann velocity distribution, and the optical frequencies experienced by moving atoms are Doppler shifted. As a result, atoms in specific velocity classes can become resonant with different hyperfine levels (F'=3, 4, 5) of the intermediate $6P_{3/2}$ state and satisfy the corresponding two-photon resonance conditions when their Doppler shifts are taken into account, giving rise to multiple EIT peaks. For example, when the probe frequency is locked to the $6S_{1/2}(F=4) \rightarrow 6P_{3/2}(F'=5)$ transition, atoms with zero velocity are excited to the $6P_{3/2}(F'=5)$ state, leading to the EIT peaks corresponding to the $6P_{3/2}$ $(F'=5) \rightarrow 50D_{3/2}$ and $6P_{3/2}$ $(F'=5) \rightarrow 50D_{5/2}$ transitions. Meanwhile, due to the Doppler effect, atoms moving along the probe-beam direction with a velocity v = 214 m s^{-1} are also populated in the $6P_{3/2}$ (F'=4) state (the corresponding Doppler shift is $\Delta\nu = \nu_0 v / c$ = 251.092 MHz, where ν_0 is the probe frequency and c is the speed of light). Because of the wavelength mismatch between the probe and coupling beams, these atoms with the specific velocity experience a Doppler shift of 251.092 × (852.356/509.627) ≈ 420.0 MHz for the coupling laser. Under the two-photon resonance condition, this gives rise to the EIT signal A in figure 4, corresponding to the $6P_{3/2}$ $(F'=4) \rightarrow 50D_{5/2}$ transition. Since the experiment is performed in the counter-propagating configuration, the frequency interval between this signal A and the $6P_{3/2}$ $(F'=5) \rightarrow 50D_{5/2}$ EIT resonance is 420.0 - 251.1 = 168.9 MHz. The red solid curve in figure 4(c) represents the theoretical Rydberg EIT spectra calculated using equation (4) by integrating over one-dimensional velocity distribution of thermal atoms, which agrees well with the experimental data, represented by the blue dotted points. As discussed above, this interval is determined primarily by the hyperfine splitting of the intermediate $6P_{3/2}$ state and the wavelengths of the probe and coupling lasers. It therefore provides a stable and reliable intrinsic frequency ruler for calibrating the Rydberg EIT spectra without requiring any additional frequency-reference device, thereby significantly simplifying the experimental setup. Using this intrinsic frequency ruler, the fine-structure splitting of the 50D state is measured to be 565 ± 4 MHz, in agreement with the value obtained using the EOM calibration method within ~1.0%, confirming the reliability of this frequency-calibration approach. In fact, this method can also be extended to microwave electric-field measurements through the A-T splitting of nS/nD Rydberg states.

We further investigate the influence of the frequency detuning of the 852 nm probe laser on the spectral characteristics of Rydberg EIT. In the experiment, the probe laser is locked to different resonance and crossover peaks in the SAS at the $6S_{1/2}(F=4) \rightarrow 6P_{3/2}$ transition, while the 510 nm coupling laser is scanned across the $6P_{3/2} \rightarrow 50D$ transition, and the corresponding Rydberg EIT signals are shown in figure 5. As discussed above for EIT signal A in figure 4, when the Doppler effect is taken into account, six EIT peaks should be expected under the two-photon resonance condition. From low to high frequency, these peaks correspond to the $6P_{3/2}(F'=3, 4, 5) \rightarrow 50D_{3/2}$ and $6P_{3/2}(F'=3, 4, 5) \rightarrow 50D_{5/2}$ transitions, respectively. All six EIT

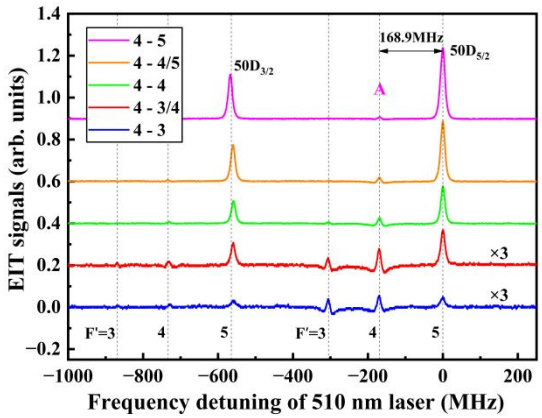


Figure 5. Rydberg EIT spectra obtained with the 852 nm probe laser locked to different resonance and crossover peaks in the SAS at the $6S_{1/2}$(F=4) and $6P_{3/2}$(F'=3,4,5) transitions.

peaks can be clearly observed in the Rydberg spectra as shown in figure 5, particularly when the probe laser is locked to the $6S_{1/2}$(F=4) → $6P_{3/2}$(F'=3/4) crossover resonance. Varying the probe laser detuning results only in relative changes in the amplitudes of the Rydberg EIT peaks and an overall spectral shift, while the frequency separations between these EIT peaks remain unchanged. When the $6P_{3/2}$ (F'=5) → $50D_{5/2}$ EIT signals measured at different probe laser frequencies are taken as the zero-detuning reference, the EIT peaks corresponding to the same transitions are approximately aligned, as indicated by the vertical dashed lines in figure 5. This result demonstrates that the frequency intervals in the Rydberg EIT spectra are insensitive to variations in the probe frequency detuning, thereby facilitating precise interval measurements using the intrinsic frequency scale. When the probe frequency is locked to different positions in the SAS, its detuning relative to the individual $6S_{1/2}$(F=4) → $6P_{3/2}$(F'=3,4,5) hyperfine transitions changes accordingly. As a result, atoms with different velocity classes are selectively excited, leading to a redistribution of the effective populations among the $6P_{3/2}$(F'=3,4,5) hyperfine states. This redistribution, in turn, modifies the intensities of the EIT peaks associated with the $6P_{3/2}$ (F'=3, 4, 5) → $50D_{3/2}$ and $50D_{5/2}$ transitions.

3.2. Comparison of Rydberg spectra under counter- and co-propagating beam configurations

Rydberg states are characterized by large principal quantum numbers and intrinsically narrow natural linewidths, and efficient excitation is challenging whether atoms are driven directly from the ground state to a Rydberg state by a single-photon excitation scheme [20, 21], or excited from the ground state to a Rydberg state via an intermediate state in a two-photon excitation scheme [10-17]. Consequently, relatively strong coupling fields are generally required, often generated through nonlinear frequency conversion with an output power on the order of hundreds of mW [17, 20, 21, 35]. In the present experiment, the 510 nm coupling beam is provided by an ECDL with a maximum output power of only 30 mW. To increase the intensity of coupling laser, a convex lens with a focal length of 75 mm is used to focus the beam to the center of Cs vapor cell. With the aid of ladder-type EIT effect, Rydberg EIT spectra with a reasonably good SNR are obtained in the counter-propagating configuration. However, theoretical calculations based on equation (4) predict that Doppler broadening significantly suppresses the EIT signal in the co-propagating configuration, as shown in figure 2. Surprisingly, during the experiment, when the Cs cell is oriented normal to the incident 510 nm coupling beam, partial reflection of the 510 nm beam occurs at the cell window. The reflected 510 nm beam and the 852 nm probe beam then form a co-propagating configuration inside the Cs cell, under which a measurable Rydberg spectral signal is observed. Motivated by this observation, the co-propagating and counter-propagating configurations as shown in figure 3

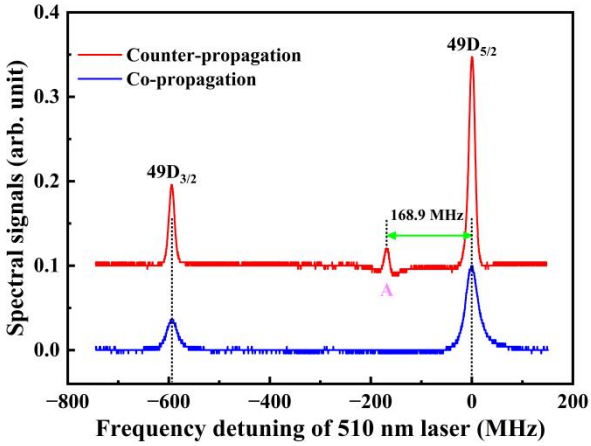


Figure 6. Comparison of the Rydberg atomic spectra for counter- and co-propagating probe and coupling beams in the Cs vapor cell.

are implemented experimentally, and rapid switching between the two geometries is achieved by blocking the 510 nm coupling beam before DM1 or DM2. Under identical conditions (probe power: 2.8 μW; coupling power: 30 mW), the Rydberg spectra obtained in the two configurations are systematically compared, with a typical result shown in figure 6. Compared with the co-propagating geometry, the counter-propagating configuration yields Rydberg EIT spectra with a larger signal amplitude and a narrower linewidth. Nevertheless, in the co-propagating configuration, well-resolved Rydberg spectral signals can still be obtained, even when the ladder-type EIT effect is significantly suppressed. In this geometry, moving atoms experience Doppler shifts from the probe and coupling lasers in the same direction. Consequently, peak A, corresponding to the $6P_{3/2}$ (F'=4) → $49D_{5/2}$ transition, is shifted to the high-frequency side of the $6P_{3/2}$ (F'=5) → $49D_{5/2}$ resonance, and therefore lies outside the spectral range shown in the figure 6. A similar analysis has been applied to figure 4(c).

As the coupling power increases from 2.5 mW to 30.0 mW, the amplitudes of the Rydberg spectral signals corresponding to the $6P_{3/2}$ (F'=5) → $49D_{5/2}$ transition initially increase and then approach saturation in both configurations. The full width at half maximum (FWHM) in both configurations increases slowly with increasing power. Specifically, in the counter-propagating configuration, the FWHM increases from about 10 MHz to 13 MHz, whereas in the co-propagating configuration it increases from about 20 MHz to 26 MHz, as shown in figure 7.

The linewidths of Rydberg atomic spectra arises from multiple contributions, including the natural linewidths of the atomic levels, laser linewidths, power broadening, collisional broadening, Doppler broadening and so on. When the 852 nm probe laser is resonant with the ^{133}Cs $6S_{1/2}$(F=4) → $6P_{3/2}$(F'=5) transition, it predominantly transfers atoms with velocity components near $v \approx 0$ from the ground state $6S_{1/2}$(F=4) to the intermediate state $6P_{3/2}$(F'=5). The corresponding velocity range δv can be approximately expressed as:

$$\frac{\delta v}{c} \cdot \nu_{852} = \Gamma_2 \sqrt{1 + I_{852}/I_{sat}} \tag{5}$$

where ν_{852} is the frequency of the probe laser, $\Gamma_2 = 5.2$ MHz is the natural linewidth of the intermediate state $6P_{3/2}$, and I_{sat} is the saturation intensity of the $6S_{1/2} \rightarrow 6P_{3/2}$ transition. Since the average intensity of the 852 nm probe laser I_{852} is relatively low over the entire length of the Cs vapor cell, its power broadening can be neglected. Thus, equation (5) gives:

$$\delta v = \lambda_{852} \cdot \Gamma_2 \tag{6}$$

Atoms in the intermediate state $6P_{3/2}$ are further excited to the Rydberg state nD by the 510 nm coupling laser. Similarly, only atoms with velocity components within the range δv contribute to the Rydberg spectrum. For the counter-propagating configuration, the residual Doppler broadening is given by [36, 37]:

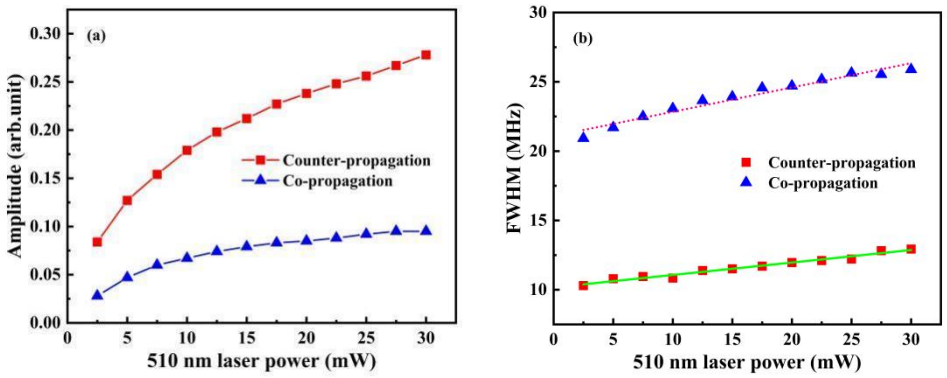


Figure 7. Dependence of the amplitude (a) and FWHM (b) of the Rydberg atomic spectral signals on the power of the 510 nm coupling beam for the counter- and co-propagating configurations. The solid lines in figure 7(b) represent linear fits.

$$\Delta\nu_{CTP} = \left|\frac{1}{\lambda_{510}} - \frac{1}{\lambda_{852}}\right| \cdot \delta v = 3.5\ \text{MHz} \tag{7}$$

whereas for the co-propagating configuration, the Doppler broadening is:

$$\Delta\nu_{CP} = \left|\frac{1}{\lambda_{510}} + \frac{1}{\lambda_{852}}\right| \cdot \delta v = 14.1\ \text{MHz} \approx 4\Delta\nu_{CTP} \tag{8}$$

The power broadening induced by the 510 nm coupling laser is written as [37]:

$$\Delta\nu_{510} = (\Gamma_{nD} + \Gamma_2) \cdot \sqrt{1 + I_{510}/I'_{sat}} \tag{9}$$

where $\Gamma_{49D} \approx 3.8$ kHz is the natural linewidth of the Rydberg state $49D_{5/2}$ [7, 38], and I'_{sat} is the saturation intensity of the $6P_{3/2} \rightarrow 49D_{5/2}$ transition, which is approximately $10^3 \sim 10^4$ mW / cm^2 [7]. Other spectral broadening denoted by $\Delta\nu_{other}$, originates from collisional broadening, stray electromagnetic-field broadening, and related effects. Since the experimentally measured Rydberg spectra are close to a Lorentzian profile as shown in figure 6, the total linewidth can be estimated, for simplicity, as [37]:

$$\Delta\nu_{obs} = \Delta\nu_{510} + \Delta\nu_{other} + \Delta\nu_{CTP}(\Delta\nu_{CP}) \tag{10}$$

Substituting equation (9) into equation (10) yields:

$$\Delta\nu_{obs} = (\Gamma_{nD} + \Gamma_2) \cdot \sqrt{1 + \alpha \cdot P_{510}} + \Delta\nu_{other} + \Delta\nu_{CTP}(\Delta\nu_{CP}) \tag{11}$$

where P_{510} is the power of coupling laser and α is a fitting coefficient. Because the saturation intensity of the $6P_{3/2} \rightarrow 49D$ transition is relatively large, $\alpha \cdot P_{510}$ remains a small quantity when the coupling laser power is below 30 mW in experiment. Therefore, equation (11) can be expanded in a Taylor series as:

$$\Delta\nu_{obs} = (\Gamma_{nD} + \Gamma_2) \cdot (1 + \alpha \cdot P_{510}/2) + \Delta\nu_{other} + \Delta\nu_{CTP}(\Delta\nu_{CP}) \tag{12}$$

Using equation (12) to linearly fit the experimental data in figure 7(b), the common broadening contribution $\Delta\nu_{other}$ is obtained to be ~1.3 MHz. The residual Doppler broadening $\Delta\nu_{CTP}$ is ~3.7 MHz for the counter-propagating configuration, and $\Delta\nu_{CP}$ is ~14.6 MHz for the co-propagating configuration. The ratio of the Doppler broadening in the co- and counter-propagating configurations is ~3.9. In addition, when the power of the 510 nm coupling laser is varied from 2.5 to 30 mW, the linewidth of the Rydberg spectra changes by only 3 ~ 6 MHz, which is attributed to the relatively small variation in the corresponding saturation parameter I_{510} / I'_{sat}. In contrast, the 852 nm probe laser power has a much more pronounced influence on the spectral linewidth. According to equations (5) - (10), increasing the 852 nm laser power directly broadens the velocity range δv of atoms populated in the intermediate state $6P_{3/2}$, thereby leading to a rapid increase in the linewidth of the Rydberg spectra. Experimentally, with the 510 nm coupling laser power fixed at ~30 mW, the 852 nm probe laser power is varied from ~2.8 μW to ~1.6 mW. Even under the counter-propagating configuration, the

linewidth of the Rydberg EIT spectrum is broadened from ~10 MHz to ~81 MHz. This fact indicates that the effect of the 852 nm probe laser power on spectral broadening is significantly stronger than that of the 510 nm coupling laser power.

In the present experiment, the Rydberg spectra recorded under the co-propagating geometry remain clearly resolved, with no obvious degradation in either signal amplitude or linewidth compared with the Rydberg EIT spectra obtained in the counter-propagating configuration. Several possible mechanisms may be responsible for this behavior. One mechanism is the double-resonance optical pumping (DROP) effect, which will become more pronounced at relatively high 852 nm probe laser power [39, 40]. Another possible contribution arises from four-wave mixing (FWM) effect [23, 41, 42].

We consider DROP as a mechanism for explaining the transparency-like Rydberg spectral signal observed in the co-propagating configuration for the following reasons. (a) Although the probe power in our experiment is only 2.8 μW, the peak intensity of the probe beam at the focal point is higher than the saturation intensity of the $6S_{1/2} \rightarrow 6P_{3/2}$ transition, I_{sat} = 2.09 mW/cm^2. Consequently, a non-negligible fraction of the atoms can be transferred to the $6P_{3/2}$ intermediate excited state from the $6S_{1/2}$ (F=4) ground state. Experimentally, the observed contribution of atoms with the specific nonzero velocity groups to the Rydberg spectra provides further evidence for such optical excitation, as shown in figure 5. Subsequently, the atoms are further excited from the $6P_{3/2}$ intermediate state to the nD Rydberg state by 30 mW of coupling laser. (b) DROP is a two-photon optical-pumping process. Specifically, cesium atoms are excited from one ground-state hyperfine level, $6S_{1/2}$ (F=4), to the Rydberg nD state through a two-step transition driven by the probe and coupling fields. Importantly, the hyperfine splittings of the high-lying Rydberg states are sufficiently small that the corresponding hyperfine components are effectively unresolved. Therefore, the $nD_{3/2}$ (F" = 2-5) and $nD_{5/2}$ (F" = 1-6) states contain multiple hyperfine sublevels that can participate in the DROP process and provide multiple spontaneous-decay pathways. Atoms excited to the nD state can subsequently decay spontaneously through various intermediate excited states and eventually populate the other ground-state hyperfine level, $6S_{1/2}$ (F=3). Such population redistribution depletes the population of the $6S_{1/2}$ (F=4) state and consequently reduces the absorption of the 852 nm probe beam, producing an observable transparency-like Rydberg spectral signal. Moreover, DROP signals associated with the degenerate hyperfine levels of $nD_{5/2}$ (or $nD_{3/2}$) Rydberg state appear at the same spectral position such as the $6P_{3/2}$ (F'=5) → $nD_{5/2}$ (F" = 6,5,4) (or $6P_{3/2}$ (F'=5) → $nD_{3/2}$ (F" = 5,4)) transitions. These signals overlap with each other, resulting in enhanced transparency of the probe laser.

During two-step excitation to a Rydberg state, some additional intermediate excited states are inevitably involved, forming multiple diamond-type FWM pathways. In the co-propagating geometry, the phase-matching condition for FWM is more readily satisfied, as demonstrated experimentally [41, 42]. Moreover, Rydberg spectral signals obtained via FWM have also been reported previously [23]. Since FWM is a coherence-enhanced nonlinear optical process, it may contribute to the well-resolved Rydberg spectra observed in the co-propagating configuration.

For a ladder-type EIT, it is generally required that the probe wavelength be longer than the coupling wavelength in theory, and most two-step Rydberg excitation schemes satisfy this condition, allowing EIT induced quantum coherence to be exploited for high SNR Rydberg EIT spectroscopy, as shown by the theoretical results in figure 2. By contrast, the situation is less favorable for Rydberg EIT systems in which the probe wavelength is shorter than the coupling wavelength. For example, in 2026, Rydberg spectra have been observed by Autler-Townes splitting in the rubidium $5S_{1/2} \rightarrow 6P_{3/2} \rightarrow nS_{1/2}$ (420 nm + 1012-1026 nm) system, where the SNR of conventional "Rydberg EIT" is poor in a counter-propagating geometry [24]. For such inverted systems, the co-propagating configuration may provide a promising approach for improving the SNR of Rydberg spectra.

4. Conclusion

Rydberg spectra are investigated based on the ^{133}Cs $6S_{1/2} \rightarrow 6P_{3/2} \rightarrow$ nD ladder-type system using a two-photon excitation scheme. By optimizing the frequency-scanning scheme and accounting for the contributions from different atomic velocity groups, we establish an intrinsic frequency ruler for measuring spectral intervals without requiring additional optical frequency-reference devices. The reliability of this approach is validated by measuring the fine-structure splittings of the (nD) Rydberg states with an accuracy of ~1%. This frequency-calibration method can also be extended to microwave electric-field measurements based on the A-T splitting of nS/nD Rydberg states, offering a simplified experimental scheme. Furthermore, well-resolved Rydberg spectra are also obtained in the co-propagating geometry mainly due to the DROP contribution, providing greater flexibility in experimental implementation. This configuration may be advantageous for the inverted ladder-type systems ($\lambda_P < \lambda_C$), for which the ladder-type EIT is strongly suppressed in the counter-propagating configuration due to Doppler mismatch. These results may facilitate the development of compact Rydberg-spectroscopy platforms based on the co-propagating configuration, in which multiple laser fields can be delivered through a single optical fiber [29], broadening the applicability of Rydberg-based techniques to microwave detection, and quantum technologies.

Acknowledgements

Funding for this research was supported by the National Natural Science Foundation of China (NSFC Grant Nos. 12474483 and 61975102).

Author Contributions

Han Jiaofeng measured the experimental data and drafted the initial manuscript; the contributions of the other authors were equal.

Declarations

Conflict of interest The authors declare no competing interests.

References

[1] Gallagher T F 1988 Rydberg atoms *Rep. Prog. Phys.* **51** 143-88
[2] Jiao Y C, Han X X, Yang Z W, Li J K, Raithel G, Zhao J M and Jia S T 2016 Spectroscopy of cesium Rydberg atoms in strong radio-frequency fields *Phys. Rev. A* **94** 023832
[3] Fields G, Dunning F B, Yoshida S and Burgdörfer J 2019 Destruction of high-n (n ~ 300) Rydberg atoms in Rydberg-Rydberg collisions *Phys. Rev. A* **99** 022710
[4] Zhou F, Jia F D, Mei J, Liu X B, Zhang H Y, Yu Y H, Liang W C, Qin J W, Zhang J, Xie F and Zhong Z P 2022 The effect of the Doppler mismatch in microwave electrometry using Rydberg electromagnetically induced transparency and Autler-Townes splitting *J. Phys. B: At. Mol. Opt. Phys.* **55** 075501
[5] Zhao J M, Zhu X B, Zhang L J, Feng Z G, Li C Y and Jia S T 2009 High sensitivity spectroscopy of cesium Rydberg atoms using electromagnetically induced transparency *Opt. Express* **17** 15821-26
[6] Bao S X, Zhang H, Zhou J, Zhang L J, Zhao J M, Xiao L T and Jia S T 2016 Polarization spectra of Zeeman sublevels in Rydberg electromagnetically induced transparency *Phys. Rev. A* **94** 043822
[7] Bhowmik A, Gaudesius M, Biedermann G and Blume D 2024 Double, triple, and quadruple magic wavelengths for cesium ground, excited, and Rydberg states *Phys. Rev. A* **110** 043114
[8] Mohapatra A K, Jackson T R and Adams C S 2007 Coherent optical detection of highly excited Rydberg states using electromagnetically induced transparency *Phys. Rev. Lett.* **98** 113003

[9] Yang B D, Gao J, Zhang T C and Wang J M 2011 Electromagnetically induced transparency without a Doppler background in a multilevel ladder-type cesium atomic system *Phys. Rev. A* **83** 013818
[10] Pei D L, He J, Wang J Y, Wang J C and Wang J M 2017 Measurement of the fine structure of cesium Rydberg state *Acta Phys. Sin.* **66** 193701
[11] Jiao Y C, Hao L P, Han X X, Bai S Y, Raithel G, Zhao J M and Jia S T 2017 Atom-based radio-frequency field calibration and polarization measurement using cesium nD_J floquet states *Phys. Rev. Appl.* **8** 014028
[12] Silpa B S, Barik S K, Chaudhuri S and Roy S 2022 Transition frequency measurement of highly excited Rydberg states of ^{87}Rb for a wide range of principal quantum numbers *Opt. Continuum* **1** 1176-92
[13] Bao S X, Zhang H, Zhang L J, Xiao L T and Jia S T 2024 Measurement of relative transition strengths of ^{133}Cs Rydberg D states using electromagnetically induced transparency *Sci. Rep.* **14** 7779
[14] Chang R, Wang T, Yang Y H, Hao L L, He J and Wang J M 2025 Effect of the coupling beam with different intensity profile upon Rydberg EIT and Rydberg two-color polarization spectroscopy with cesium ladder-type level *Adv. Quantum Technol.* **8** 2400469
[15] Prajapati N, Robinson A K, Berweger S, Simons M T, Artusio-Glimpse A B and Holloway C L 2021 Enhancement of electromagnetically induced transparency based Rydberg-atom electrometry through population repumping *Appl. Phys. Lett.* **119** 214001
[16] Su H J, Liou J Y, Lin I C and Chen Y H 2022 Optical pumping effects on high-contrast Rydberg electromagnetically induced transparency *J. Appl. Phys.* **132** 244401
[17] Wang Q X, Wang Z H, Liu Y X, Guan S J, He J, Zhang P F, Li G and Zhang T C 2023 Cavity-enhanced spectra of hot Rydberg atoms *Acta Phys. Sin.* **72** 087801
[18] Wang Q X, Liang Y K, Wang Z H, Guan S J, Yang P F, Zhang P F, Li G and Zhang T C 2025 High-precision measurement of microwave electric field by cavity-enhanced critical behavior in a many-body Rydberg atomic system *Sci. China Phys. Mech. Astron.* **68** 264211
[19] Liu B, Zhang L H, Wang Q F, Ma Y, Han T Y, Liu Z K, Zhang Z Y, Shao S Y, Zhang J, Li Q, Chen H C, Han Y L, Ding D S and Shi B S 2025 Cavity-enhanced Rydberg atom microwave receiver *Chin. Phys. Lett.* **42** 053201
[20] Li B, Li M, Jiang X J, Qian J, Li X L, Liu L and Wang Y Z 2019 Optical spectroscopy of nP Rydberg states of ^{87}Rb atoms with a 297-nm ultraviolet laser *Phys. Rev. A* **99** 042502
[21] Liu S, Bai J D, Wang J Y, He J and Wang J M 2019 Measurement of quantum defect of cesium $nP_{3/2}$ (n = 70-94) Rydberg states by using ultraviolet single-photon Rydberg excitation *Acta Phys. Sin.* **68** 073201
[22] Duspayev A and Raithel G 2025 Hyperfine structure and collisions in three-photon Rydberg electromagnetically induced transparency *Phys. Rev. A* **111** 032821
[23] de Melo N R and Vianna S S 2014 Two-photon resonant forward four-wave mixing in rubidium vapor involving Rydberg states *J. Opt. Soc. Am. B* **31** 1735-40
[24] Xiang T, Lu Y H, Ho J, Lee T C, Yan Z J and Stamper-Kurn D M 2026 Autler-Townes spectroscopy of a Rydberg ladder *Phys. Rev. A* **113** 013126
[25] Mack M, Karlewski F, Hattermann H, Höckh S, Jessen F, Cano D and Fortágh J 2011 Measurement of absolute transition frequencies of ^{87}Rb to nS and nD Rydberg states by means of electromagnetically induced transparency *Phys. Rev. A* **83** 052515
[26] Shen P R, Pawlak M, Booth D, Nickerson K, Miladi H, Sadeghpour H R and Shaffer J 2025 Precision measurement of $Cs(nF_J)$ quantum defects and calculations of scalar and tensor polarizabilities of the $nS_{1/2}$, nP_J, nD_J, and nF_J series *Phys. Rev. A* **112** 022814
[27] Su K, Behary R, Aubin S, Mikhailov E E and Novikova I 2025 Two-photon Rydberg EIT resonances in non-collinear beam configurations *J. Opt. Soc. Am. B* **42** 757-62
[28] Ren S, Tang Y, Yang C, Wang S Y and Zhou H B 2024 Accurate measurement of the frequency offset of the laser based on electromagnetically induced transparency *Appl. Opt.* 63 4219-25
[29] Yin Y W, Chen R M, Ji S B, Hu J L, Wang S F, He Y H, Bai J X, Shao X Q, Jiao Y C and Zhao J M 2026 Doppler-enhanced superheterodyne Rydberg microwave receiver *Appl. Phys. Lett.* **129** 014003
[30] Gea-Banacloche J, Li Y Q, Jin S Z and Xiao M 1995 Electromagnetically induced transparency in ladder-type inhomogeneously broadened media: Theory and experiment *Phys. Rev. A* **51** 576-84
[31] Finkelstein R, Bali S, Firtenberg O and Novikova I 2023 A practical guide to electromagnetically induced transparency in atomic vapor *New J. Phys.* 25 035001
[32] Urvoy A, Carr C, Ritter R, Adams C S, Weatherill K J and Löw R 2013 Optical coherences and wavelength mismatch in ladder systems *J. Phys. B: At. Mol. Opt. Phys.* **46** 245001
[33] Zhang L D, Stiesdal N, Busche H, Hansen M G, Pohl T and Hofferberth S 2024 Interplay of electromagnetically induced transparency and Doppler broadening in hot atomic vapors *New J. Phys.* 26 075002
[34] Shen P R, Booth D, Liu C, Beattie S, Marceau C, Shaffer J P, Pawlak M and Sadeghpour H R 2024 Ultraprecise determination of $Cs(nS_{1/2})$ and $Cs(nD_J)$ quantum defects for sensing and computing: evaluation of core contributions *Phys. Rev. Lett.* **133** 233005
[35] Liu Y, He J, Su N, Cai T, Liu Z H, Diao W T and Wang J M 2023 A 509 nm pulsed laser system for Rydberg excitation of cesium atoms *Acta Phys. Sin.* **72** 060303
[36] Tanasittikosol M, Carr C, Adams C S and Weatherill K J 2012 Subnatural linewidths in two-photon excited-state spectroscopy *Phys. Rev. A* **85** 033830

[37] Bransden B H and Joachain C J 2003 Physics of atoms and molecules *Essex, England: Prentice Hall*
[38] Du J Q, Gong T, Ji Z H, Wang C H, Zhao Y T, Xiao L T and Jia S T 2021 Radiative lifetime measurement of ultracold cesium Rydberg states by a simplified optical pumping method *Appl. Opt.* **60** 276-80
[39] Yang B D, Liu Y and Wang J M 2020 Double resonance optical pumping-polarization spectroscopy of an excited state transition *Opt. Commun.* **474** 126102
[40] Moon H S, Lee W K, Lee L and Kim J B 2004 Double resonance optical pumping spectrum and its application for frequency stabilization of a laser diode *Appl. Phys. Lett.* **85** 3965-67
[41] Schultz J T, Abend S, Döring D, Debs J E, Altin P A, White J D, Robins N P and Close J D 2009 Coherent 455 nm beam production in a cesium vapor *Opt. Lett.* **34** 2321-23
[42] Gai B D, Hu S, Chu J Z, Wang P Y, Cai X L and Guo J W 2021 Collimated ultraviolet light generated by four-wave mixing process in Cs vapor *OSA Continuum* **4** 2410-22